CATALYSIS FOR SUSTAINABLE ENERGY
Research Article • DOI: 10.2478/cse-2012-0002 • CSE • 2013 • 11–21

VERSITA

Steam reforming of methane over Ni-substituted Sr hexaaluminates.

Abstract
Ni-substituted Sr-aluminates $Sr_{1-x}Ni_xAl_{11.2+x}Ni_{0.8-x}O_{19-\delta}$ (x = 0; 0.2; 0.4; 0.8) obtained by a precipitation method and calcined at 1200°C have been characterized by different physicochemical techniques and their catalytic properties have been tested in steam reformation of methane. It has been shown that substitution of Al^{3+} and/or Sr^{2+} by Ni^{2+} in the aluminate structure results in changes of phase composition, specific surface area, and reducibility of samples. It has been established that the samples are not completely reduced in the temperature range of 30–900°C. The $Sr_{1-x}Ni_xAl_{11.2+x}Ni_{0.8-x}O_{19-\delta}$ (x = 0; 0.2; 0.4) catalysts are active and stable in the steam reforming of methane at 700oC: residual amount of methane is (1.1±1.0) vol.%, while the $Sr_{1-x}Ni_xAl_{11.2+x}Ni_{0.8-x}O_{19-\delta}$ (x = 0.8) sample is rapidly deactivated by coking.

Keywords
Ni-substituted aluminates • Steam reforming • Methane • Catalyst

Marina V. Bukhtiyarova[1,2*], Aleksandra S. Ivanova[1], Elena M. Slavinskaya[1], Pavel A. Kuznetsov[1], Lyudmila M. Plyasova[1], Olga A. Stonkus[1], Vladimir A. Rogov[1], Vasilii V. Kaichev[1], Aleksandr S. Noskov[1]

[1]Boreskov Institute of Catalysis, Pr. Akademika Lavrentieva 5, 630090, Novosibirsk, Russian Federation

[2]Novosibirsk State University, Str. Pirogova 2, 630090, Novosibirsk, Russian Federation

Received 16 April 2012
Accepted 29 May 2012

1. Introduction

Natural gas, specifically methane, is one of the most important and available energy resources [1]. Catalytic steam reforming of methane (SRM) is well-established process for converting hydrocarbons into synthetic gas in industry. The SRM is currently the most cost effective and highly developed method for production of hydrogen.

$$CH_4 + H_2O = CO + 3H_2;\ \Delta H_{298}^0 = 206\ kJ/mol$$

The SRM process is highly endothermic, and the reaction requires high temperatures of 700 – 800°C [1,2]. Besides, the reaction is always followed by the water gas shift reaction (WGS) yielding CO_2 as by-product

$$CO + H_2O = CO_2 + H_2;\ \Delta H_{298}^0 = -41\ kJ/mol$$

It should be noted that H_2O/CH_4 ratio influences product composition. In particular, an excess amount of steam prevents coking of the catalyst surface. At the same time, high reaction temperatures and the use of excess steam increase the amount of energy consumed and, consequently, the hydrogen production cost. The development of new more active steam reforming catalysts with a high coking stability is required [3].

Supported noble metals Pd and Pt have successfully been employed as highly active catalysts for steam reforming of methane to synthesis gas [4]; however, their industrial application is not reasonable due to their high price. Traditional supported nickel catalysts have also been reported to be effective for this reaction, but they suffer from serious deactivation due to carbon deposition, nickel particles sintering and phase transformation. Therefore, it is very important to improve the state of the Ni catalyst in order to overcome these disadvantages [5].

Among different catalysts, nickel supported on inexpensive, thermally stable α-alumina has been widely employed as the conventional industrial steam reforming catalyst [6]. Alumina is widely used as an oxide support, but its surface area significantly decreases with the transition from metastable γ-phase into the α-phase. A high surface area is desired to maintain high dispersion of catalytic components. Some researchers have greatly enhanced the catalytic activity and stability of Ni catalysts by adding some components to the alumina support to inhibit sintering and phase transformation. Basic oxide additives, such as CaO, MgO, La_2O_3, BaO, have been reported to aid in maintaining catalytic activity and suppressing the deactivation, owing to the interaction between NiO and supports [3].

The use of hexaaluminates $AAl_{12}O_{19}$ in the development of high temperature catalytic systems has been of interest primarily due to their high sintering stability [7]. Their high thermal stability is related to the lamellar structure that consists of Al_2O_3-containing spinel block, intercalated by mirror planes, in which the large cations (Ba, Sr, La, etc.) are located (Figure 1) [8]. The substitution of catalytically active metals into the lattice of hexaaluminate compounds is an area of active interest of reforming catalyst applications.

* *E-mail: buhtiyarova@mal.ru*

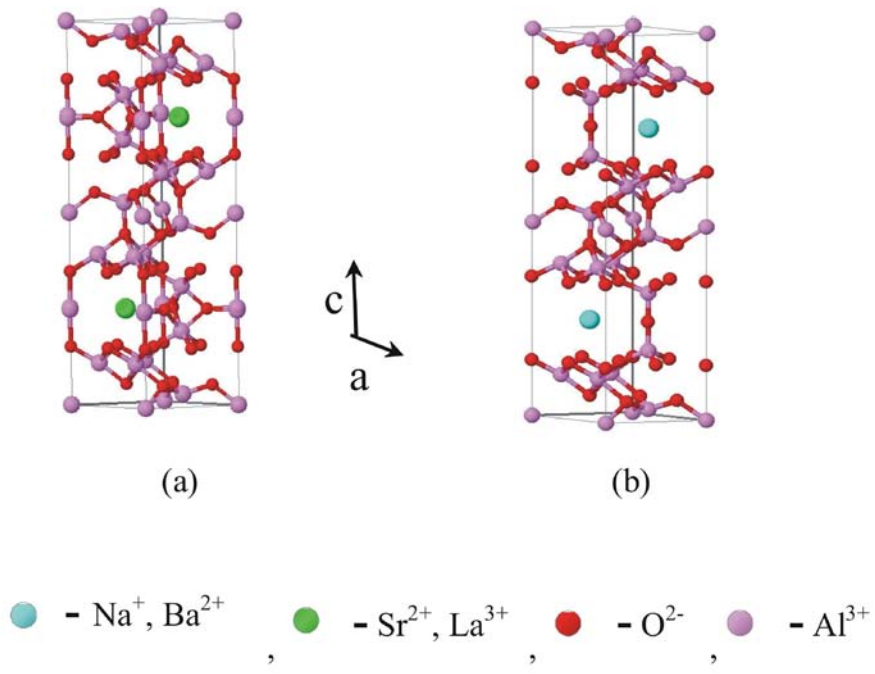

Figure 1. Crystal structure: (a) magnetoplumbite, (b) β-Al_2O_3.

One of the factors influencing activity of $ANiAl_{11}O_{19}$ catalysts in SRM can be precursor containing nickel as homogeneously dispersed component in the composition. According to [9], the reduction of such compositions results in formation of highly dispersed metal nickel on the surface of hexaaluminates.

The main requirement for the SRM catalysts is providing a high conversion of hydrocarbons at relatively low temperatures [10]. Here, we used Ni-substituted strontium hexaaluminate ($SrO{\cdot}6Al_2O_3$) with high thermal stability and high surface area as the support material. Due to the formation of a hexaaluminate phase, strontium hexaaluminate exhibited excellent heat resistance against sintering at high temperatures. Nickel ions have been introduced using mixed solution of $Ni(NO_3)_2$ and $Al(NO_3)_3$ or mixed solution of $Ni(NO_3)_2$ and $Sr(NO_3)_2$. The aim of the present work is to study the influence of the substitution of strontium and/or aluminum ions by nickel ions on phase composition, specific surface area, reducibility of aluminates, surface and catalytic properties of Ni-substituted Sr-hexaaluminates in SRM.

2. Experimental Procedure

2.1. Synthesis of catalysts

Hexaaluminates $Sr_{1-x}Ni_xAl_{11.2+x}Ni_{0.8-x}O_{19-d}$ (x = 0; 0.2; 0.4; 0.8) denoted as SrNi-1 ($SrAl_{11.2}Ni_{0.8}O_{19-d}$), SrNi-2 ($Sr_{0.8}Ni_{0.2}Al_{11.4}Ni_{0.6}O_{19-d}$), SrNi-3 ($Sr_{0.6}Ni_{0.4}Al_{11.6}Ni_{0.4}O_{19-d}$), SrNi-4 ($Sr_{0.2}Ni_{0.8}Al_{12}O_{19-d}$), were obtained by precipitation with NH_4HCO_3 from the aqueous solutions of nitrates of (Al + Ni) and Sr or Al and (Sr + Ni) at pH 7.3 – 7.5 and temperature of 70°. The slurry was aged at these conditions for two hours. The obtained precipitate was washed and dried in air at 110°C for 12 – 14 hours and then calcined at 700°C for 4 hours in air flow [11,12]. The subsequent calcination of samples was carried out at 1200°C for 4 hours in a muffler.

The Ni-containing supported catalyst (8 wt.% NiO/Mg-Al-O, support Mg-Al-O was calcined at 1200°C) prepared by impregnation of support by $Ni(NO_3)_2$ solution followed by treatment at 500°C for 4 hours was used for comparison [13].

2.2. Catalyst characterization

Elemental analysis was performed using the inductively couple plasma (ICP) - atomic absorption spectroscopy with an accuracy of 0.01 – 0.03% [14].

XRD studies were carried out using a URD-63 (Germany) diffractometer with CuK_a (λ = 1.5418 Å) monochromatic radiation. Diffraction profiles were recorded both in a continuous mode and in a step-by-step scanning mode at 0.05-0.1° in 2θ-step and dwell time of 20-30 sec depending on the crystallinity of a sample. The phase identification was performed by comparison of the measured set of the interfacial distances d_i and the corresponding intensities of the diffraction maxima I_i with those found in the database JCPDS (PCPDF Win. Ver 1.30, JCPDS ICDD, Swarthmore, PA, USA, 1997).

The specific surface area was determined with an accuracy of ±10% by the argon thermal desorption [15].

Temperature-programmed reduction (TPR) of samples by hydrogen was carried out in the flow reactor. The samples of 0.2 g with the average granule size of 0.25-0.5 mm were previously pretreated in oxygen at 500°C for 30 minutes, and then they were cooled to room temperature. The 10 vol.% H_2/Ar stream (40 ml/min) was passed over the sample while it was heated from 40 to 900°C at the heating rate of 10°C/min.

Electron-microscopic investigations of samples were carried out using transmission electron microscope JEM-2010 (JEOL) (resolution 0.14 nm, accelerating voltage 300 kV) equipped with energy-dispersive X-ray analysis (EDX) spectrometer (EDAX Co,

resolution 140 eV). For determination of elements concentrations and their ratio, the samples were deposited on carbon support fixed on copper matrix. The samples reduced by H_2-TPR were investigated by TEM. The samples after the TPR experiment were put into TEM chamber.

X-ray photoelectron spectroscopy was applied for characterization of the surface contents of elements. XPS measurements were performed on a SPECS's spectrometer equipped with an X-ray source XR-50M with a twin Al/Ag anode, an ellipsoidal crystal monochromator FOCUS-500, and a hemispherical electron energy analyzer PHOIBOS-150. The core-level spectra were typically obtained using monochromatic MgKa radiation (*hn* = 1253.6 eV). The binding energy was calibrated using the peak of C1s (Eb = 284.8 eV). The surface contents of elements were calculated from the related XPS peak area taking into account section of photoionization of corresponding terms [16]. Deconvolution of the spectra on individual components was used for detailed analysis. The shape of the lines were fitted using Lorentz and Gauss functions and spectra were background-subtracted using a Shirley fit algorithm [17]. The samples calcined at 1200°C were investigated by XPS. Before testing the samples were additionally dried at 110°C for removal of physically adsorbed water and supported on double-sided scotch paper.

2.3. Catalyst activity

Catalytic properties of samples were investigated using setup with flow reactor and chromatographic analysis of the gas mixture. The initial catalyst was reduced at 900°C in the gas mixture of 5%H_2/He for 1.5 hours. After reduction, the reactor was purged by argon and cooled down to 700°C. The catalytic activity of reduced samples was tested using a mixture of 33 vol.% CH_4 and 66 vol.% H_2O at a total flow rate 100 ml/min. The catalyst volume was 1.0 cm^3, and space velocity was 6000 h^{-1}.

Analysis of gas composition was carried out using chromatograph "Crystal 2000M" equipped with the thermal conductivity detector. CH_4 and CO_2 concentrations were determined using column with sorbent Porapak QS (length 3 m, 35°C). CO and H_2 concentrations were determined using column with molecular sieves NaX (length 2 m, 35°C). The carrier gas was argon.

3. Results and Discussion

3.1. Phase composition and specific surface area of samples

Figure 2 and Table 1 show phase composition and specific surface area of the $Sr_{1-x}Ni_xAl_{11.2+x}Ni_{0.8-x}O_{19-d}$ (x = 0; 0.2; 0.4; 0.8) samples calcined at 1200°C. According to XRD, the SrNi-1

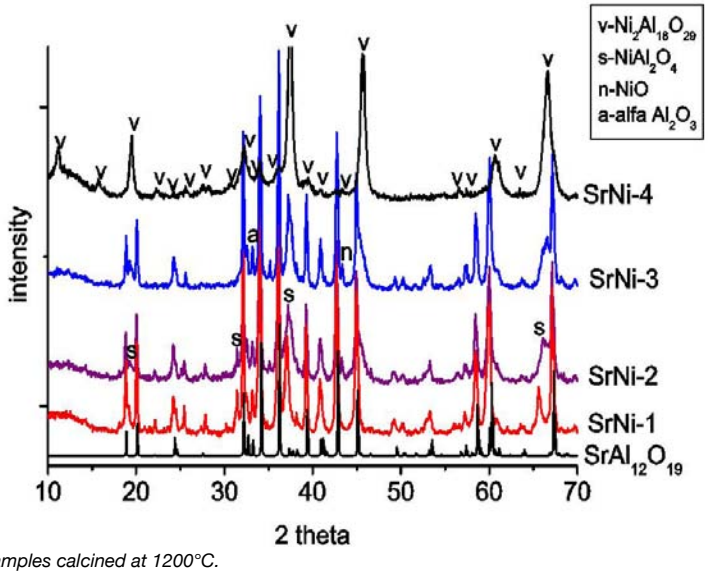

Figure 2. XRD patterns of the samples calcined at 1200°C.

Table 1. Phase composition and specific surface area of SrNi-catalysts calcined at 1200°C.

Sample	Hypothesized distribution of introduced Ni	Phase composition	S_{BET}, m^2/g
SrNi-1	$SrNi_{0.8}Al_{11.2}$	$SrAl_{12}O_{19}$, $NiAl_2O_4$, *(~ 5 вес.%)*	11
SrNi-2	$Sr_{0.8}Ni_{0.2}Ni_{0.6}Al_{11.4}$	$SrAl_{12}O_{19}$, $NiAl_2O_4$, $Ni_2Al_{18}O_{29}$, NiO, α-Al_2O_3,	21
SrNi-3	$Sr_{0.6}Ni_{0.4}Ni_{0.4}Al_{11.6}$	$SrAl_{12}O_{19}$, NiO, $Ni_2Al_{18}O_{29}$, α-Al_2O_3	20
SrNi-4	$Sr_{0.2}Ni_{0.8}Al_{12.0}$	$Ni_2Al_{18}O_{29}$	45
SrAl [19]	$SrAl_{12}O_{19}$	$SrAl_{12}O_{19}$	18

sample contains, besides main phase of hexaaluminate $SrAl_{12}O_{19}$, a small amount of nickel aluminate $NiAl_2O_4$ with the spinel structure (~ 5 wt.%). Cell parameters of a and c of hexaaluminates are 5.57 Å and 21.99 Å respectively (Table 1), *a* and *c* being smaller than standard values of Sr hexaaluminate {$SrAl_{12}O_{19}$: a=5.585 Å, c=22.07 Å; - ICDD, PDF-2, [00-026-0976]}. According to [18], the decrease of the cell parameters of hexaaluminate is observed if aluminum ions are substituted by ions with a lower oxidation state, in this case such ions are Ni^{2+} ions. Hence, during synthesis of the SrNi-1 sample of composition $SrAl_{11.2}Ni_{0.8}O_{19}$, the hexaaluminate phase doped by Ni and small amount of nickel aluminate are formed.

For the $Sr_{1-x}Ni_xAl_{11.2+x}Ni_{0.8-x}O_{19-d}$ (x = 0.2; 0.4; 0.8) samples, the increasing *x* value leads to appearance of additional phases: NiO, α-Al_2O_3, $Ni_2Al_{18}O_{29}$ and gradual decrease of amount of hexaaluminate phase (Figure 2, Table 1). For the SrNi-4 sample new phase $Ni_2Al_{18}O_{29}$ appears, the other phases are not observed. It is hypothesized that the substitution of Sr ions by Ni ions, up to x = 0.8, results in a change of Sr/Al ratio, which determines structure parameters of the hexaaluminate due to the substitution of cations with large ionic radius (Sr^{2+}: r = 1.20 Å) by cations with small one (Ni^{2+}: r = 0.74 Å) forming $Ni_2Al_{18}O_{29}$. It can be supposed that the Sr-containing phase was not observed by XRD since the lines corresponding to the $Ni_2Al_{18}O_{29}$ phase are quite broad and can be overlapped with lines of Sr-containing phase, in particular, hexaaluminate phase.

Therefore, experimental results suggest that the incorporation of nickel ions into spinel block of $SrAl_{12}O_{19}$ is a more favorable substitution preserving the hexaaluminate structure. In the case of SrNi-1, only small (5 wt.%) amount of additional phase is present, while introduction of cations into the mirror plane results in destroying hexaaluminate structure and formation of other phases (Table 1). Incorporation of nickel ions into $AAl_{12}O_{19}$ hexaaluminate structure in Al position results in the formation of hexaaluminate phase $SrAl_{12}O_{19}$. The similarity of crystal structure between Ni-substituted and unsubstituted hexaaluminates indicates that nickel ions enter hexaaluminate lattice of $SrAl_{12}O_{19}$ in basically an octahedral position. Consecutive decrease of nickel ions content in Al position and its increase in A position leads to the destruction of hexaaluminate structure and the formation of new phase that can be caused by difference in radius of Sr^{2+} and Ni^{2+} ions. As it was shown, diffractions peaks of the $SrAl_{12}O_{19}$ hexaaluminate phase overlap with those of new formed phase of $Ni_2Al_{18}O_{29}$, so it is difficult to interpret the diffractogram.

Variations of the phase composition results in changes of the specific surface area (Table 1). When strontium ions are substituted by nickel ions, the surface area increases from 18 (unsubstituted hexaaluminate) up to 45 m^2/g; when aluminum ions are substituted by nickel ions, it decreases to 11 m^2/g.

3.2. Temperature-programmed reduction by hydrogen

It is known that catalytic activity in steam reforming of methane is determined by metal nickel particles. It is assumed that interaction between reduced metal and specific structure of support are important for prevention of metal particles sintering. Therefore, the reducibility of samples by hydrogen has been investigated.

According to [20], reduction of Ni in an alumina-supported catalyst proceeds in several steps, namely: up to 400°C – reduction of bulk nickel oxide; 400 – 750°C – reduction of dispersed nickel oxide interacting with the support, 750 – 1000°C – reduction of nickel aluminates.

Figure 3 shows H_2-TPR profiles of the SrNi-1, SrNi-2, SrNi-4 samples. It is seen that SrNi-1 (curve 1) starts to reduce at 700°C with the maximum at 924°C. However reduction is not finished in the investigated temperature range. In accordance with phase composition of the SrNi-1 sample (Table 1), it can be assumed

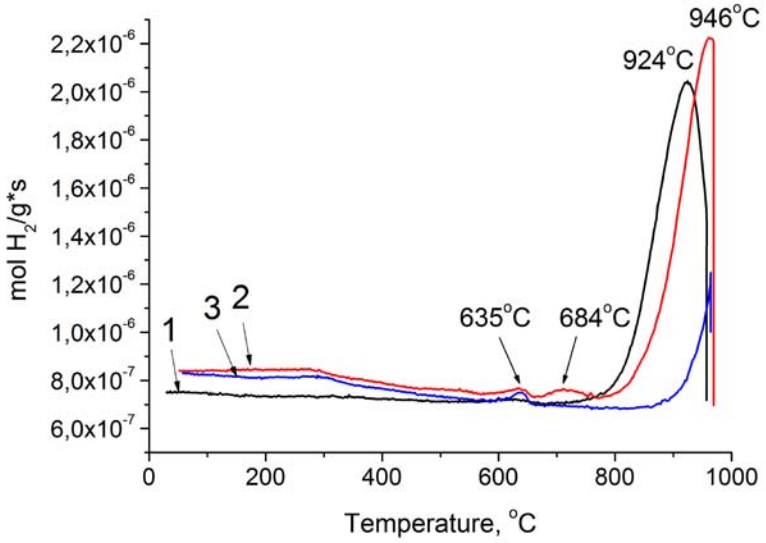

Figure 3. TPR-profiles of the (1) SrNi-1, (2) SrNi-2, (3) SrNi-4 samples calcined at 1200°C.

that nickel which is located in two phases ($NiAl_2O_4$ and $SrAl_{12}O_{19}$) is reduced that agrees with published results [21,22].

The reduction of the SrNi-2 sample proceeds in three steps with the maximums at 635, 684 and 946°C (Figure 3, curve 2). Two weak peaks at 635 and 684°C can be related to the reduction of NiO species which differ in their interaction strength with the hexaaluminate structure. The third incomplete peak at 946°C corresponds to the reduction of $NiAl_2O_4$.

The reduction of the SrNi-4 sample (Figure 3, curve 3) proceeds in two steps corresponding to reduction of NiO and, likely, $Ni_2Al_{18}O_{29}$, which is present in the sample according to XRD. At the same time reduction is not complete in the investigated temperature range. It can be concluded that nickel in samples is in strongly bonded state not reduced up to 900°C. This agrees with the literature data showing that reduction of nickel located in hexaaluminate structure proceeds at higher temperatures [21].

There is a small but noticeable trend in the temperature at which the reduction begins - the higher the degree of aluminum sites substitution by Ni, the lower the temperature at which the reduction begins. This trend suggests an increase in the concentration of less stable Ni–O–Ni bonds relative to Al–O–Ni bonds, producing slightly more reducible Ni sites. The oxygen in the mirror plane has been reported to be less strongly bound than oxygen within the spinel block which suggests that as nickel substitution of aluminum sites increases, a somewhat greater fraction of the nickel located in this region of the unit cell may be in the Ni–O–Ni environment reducing at a lower temperature than nickel present in the spinel block.

According to equation $NiO + H_2 \rightarrow Ni^0 + H_2O$, the reduction of NiO requires 13.4 mmol H_2/g. Taking into account this value, the amount of hydrogen necessary for the reduction of nickel oxide has been calculated. The calculation was carried out on the basis of concentration of NiO introduced into catalyst at the precipitation step. The amount of hydrogen consumed during reduction of SrNi-1, SrNi-2, and SrNi-4 samples was found to be 0.76, 0.91, and 0.15 mmol/$g_{catalyst}$, respectively. This is lower than calculated values of 1.09, 1.10, 1.15 mmol/$g_{catalyst}$, the highest and the lowest amounts corresponding to SrNi-2 and SrNi-4 samples, respectively. The observed difference can be related to the different bonding strength of Ni in the complex oxides, so higher temperatures are required for reduction of samples containing strongly bound Ni cations (Figure 3).

3.3. Surface distribution and states of various elements in hexaaluminates.

The surface of samples with different reducibility SrNi-1 ($SrNi_{0.8}Al_{11.2}O_{19}$), SrNi-2 ($Sr_{0.8}Ni_{0.2}Ni_{0.6}Al_{11.4}O_{19}$), and SrNi-4 ($Sr_{0.2}Ni_{0.8}Al_{12}O_{19}$) has been investigated by XPS. It has been shown that all samples contain Sr, Ni, Al, O, and C in the surface layer. Table 2 presents the results of quantitative analysis of samples surface.

As can be seen, the chemical surface composition differs from the bulk one (Table 2) as the surface of SrNi-1 and SrNi-4 samples contains a greater amount of Sr. The surface concentration of Sr in the SrNi-2 sample is slightly lower than the bulk one. For all samples the surface ratios of [Ni]/[Sr] and [Ni]/[Al] are lower than the bulk ones. It can be related to segregation of Sr and Al at the surface.

The aluminum in the samples is in an oxidized state. The Al*2p* binding energy is 74.0 – 74.4 eV that corresponds to Al^{3+} (Figure 4a). For comparison, aluminum in α-Al_2O_3 and AlOOH is characterized by the Al*2p* binding energy of 74.2 and 73.9 eV, respectively [23,24]. According to [24,25], the Al*2p* binding energy lies in the range 74.1-74.8 eV for $SrAl_{12}O_{19}$, $SrNiAl_{11}O_{19-\delta}$, $LaFeAl_{11}O_{19-\delta}$, $LaMnAl_{11}O_{19-\delta}$ hexaaluminates. The formation of Sr and Ni aluminates can be explained by monotonous increase in the Al*2p* binding energy with decrease of Sr and Ni concentrations. Spectra O*1s* (Figure 4b) show single peak at 530.9 – 531.1 eV which corresponds to the O*1s* binding energy for Al_2O_3 and $SrAl_{12}O_{19}$ (531.1 эВ).

Figure 4c shows the Sr*3d* spectra of the samples. The Sr*3d* spectrum shows the unresolved spin-orbit $Sr3d_{5/2}$ – $Sr3d_{3/2}$ doublet (intensity ratio 3:2 and splitting of ca. 1.79 eV). The Sr*3d* spectra for the samples investigated (Figure 4c) are described by two doublets with the $Sr3d_{5/2}$ binding energies of 132.8-132.9 and 133.9-134.0 eV. According to [5,24], the binding energy of strontium ions in SrO, $Sr(OH)_2$ and $SrCO_3$ is in the range of 131.7-132.4, 132.8 and 133.4-133.8 eV [25,26], respectively. This literature data allow assignment of the first doublet to Sr^{2+} in the mixed oxide Sr-Ni-Al-O and the second one – to hydroxocarbonate phase. The C*1s* spectra exhibit two peaks at 284.8 eV and 289.2-289.3 eV related to hydrocarbon admixture and carbonate groups, respectively [27]. The relative intensity of the doublet with the higher $Sr3d_{5/2}$ binding energy and C*1s* peak at 289.0 eV corresponds to the molar ratio [Sr]/[CO_3] of 1.3 – 1.7. It can be supposed that Sr is predominantly localized on the surface as $SrCO_3$. Strontium in the $SrNiAl_{11}O_{19-\delta}$ hexaaluminate phase is characterized by the $Sr3d_{5/2}$ binding

Table 2. The O1s, Al2p, $Ni2p_{3/2}$ and $Sr3d_{5/2}$ binding energies (eV) and relative concentration of metals on the sample surface.

Sample	[O]/[Me]	[Sr]/[Al]	[Ni]/[Al]	[Ni]/[Sr]	O1s	Al2p	$Ni2p_{3/2}$	$Sr3d_{5/2}$
SrNi-1	1.33 (1.46)[1]	0.29 (0.09)	0.04 (0.07)	0.15 (0.8)	530.9	74.0	855.9	132.8/ 133.9
SrNi-2	1.68 (1.46)	0.05 (0.07)	0.03 (0.07)	0.58 (1.0)	531.1	74.3	856.1	132.9/ 134.0
SrNi-4	1.60 (1.46)	0.03 (0.02)	0.01 (0.08)	0.49 (4.0)	531.3	74.4	856.4	132.8/ 134.0

[1] *stoichiometric values are given in the brackets*

energy of 133.9 [25]. Taking into account the above mentioned works, the segregation of Sr and formation of $SrCO_3$ particles on the hexaaluminate surface during synthesis is possible.

Figure 4d shows the Ni*2p* spectra of samples. Due to spin-orbit interaction, the Ni*2p* spectra are described by doublet $Ni2p_{3/2}$-$Ni2p_{1/2}$. Therefore, two narrow peaks at 855.9-856.4 and 873.5-873.9 eV are observed. Besides, the Ni*2p* spectra are characterized by additional weak shake-up satellites at 862 and 880 eV [28,29]. It is known that intensive shake-up satellites are observed in NiO, $Ni(OH)_2$, and $NiAl_2O_4$ spectra [29-31]. At the same time, the satellite structure is absent in the case of Ni^0 and Ni^{3+}. The $Ni2p_{3/2}$ binding energy for $NiAl_2O_4$, NiO, $Ni(OH)_2$, $NiSiO_3$ lies in the range of 856.2-857.2, 853.8-854.6, 855.5-855.9 and 856.3-856.7 eV, respectively [23,29-31]. Chu et al. [32] believe

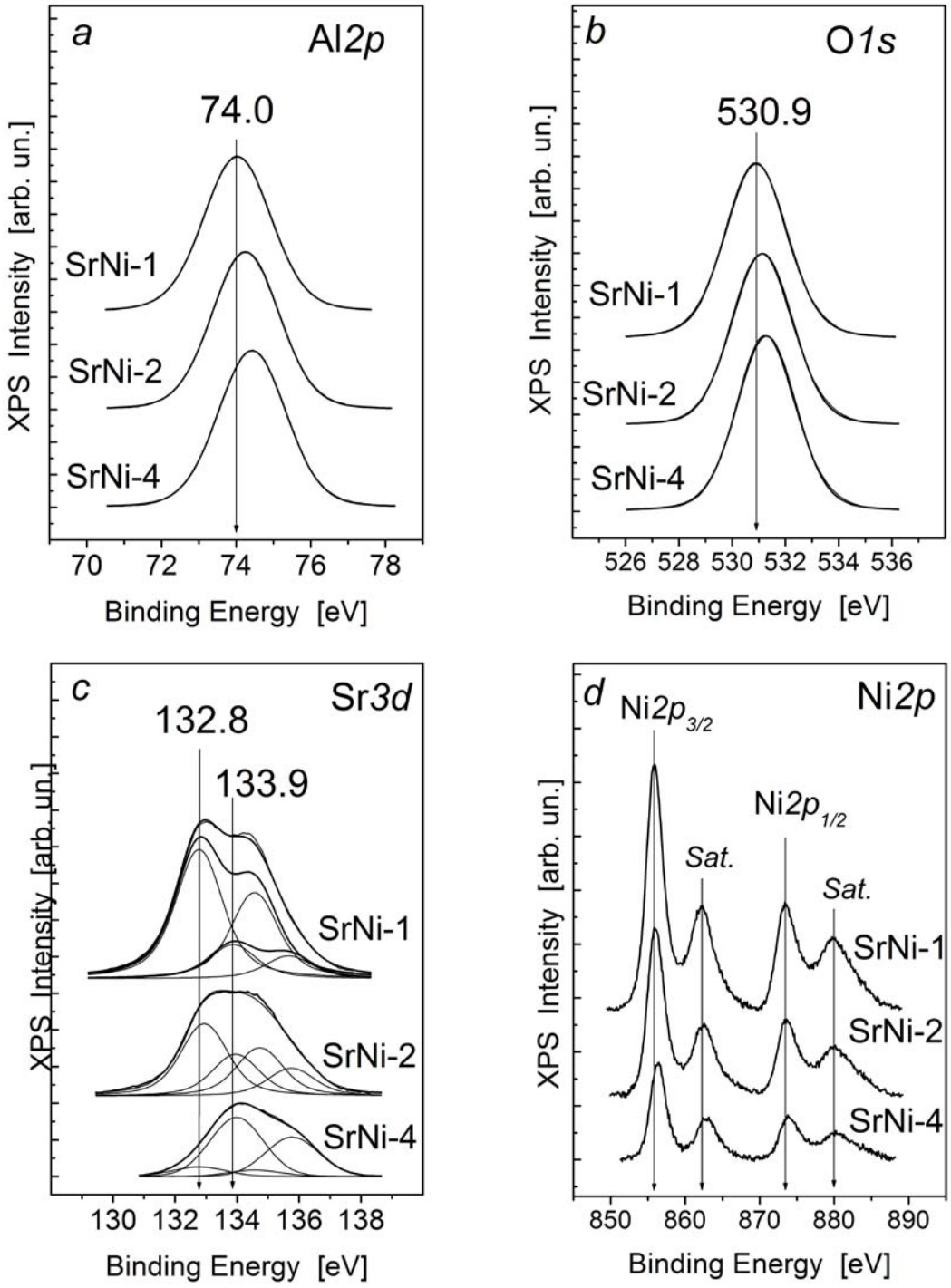

Figure 4. The Al2p (a), O1s (b), Sr3d (c), Ni2p (d) spectra of investigated samples. All spectra are normalized to the intensity of corresponding Al2p spectra.

that the Ni2$p_{3/2}$ binding energy of 856 eV together with «shake-up satellite» at 862 eV correspond to spinel $NiAl_2O_4$.

The crystal structure of Sr-hexaaluminate belongs to magnetoplumbite, which consists of alternative stacked spinel blocks and mirror planes [33]. Aluminum ions can be substituted by nickel ions in spinel block. Therefore, the Ni ion modification in the hexaaluminate is actually present in the lattices of the spinel block such as $NiAl_2O_4$ [34]. The binding energy of the Ni2$p_{3/2}$ in the hexaaluminate should be similar to that of Ni2$p_{3/2}$ in $NiAl_2O_4$. Therefore, it is reasonable to attribute the peak at 856.4 eV to Ni^{2+} in spinel $NiAl_2O_4$ and hexaaluminate $SrAl_{12}O_{19}$ structures, modified by Ni ions that is confirmed by XRD. For the SrNi-4 sample the Ni2$p_{3/2}$ binding energy of 856.4 eV corresponds to Ni^{2+} in the mixed oxide.

3.4. Catalytic activity of Ni-substituted Sr-hexaaluminates

Catalytic properties of SrNi-1 ($SrAl_{11.2}Ni_{0.8}O_{19-d}$), SrNi-2 ($Sr_{0.8}Ni_{0.2}Al_{11.4}Ni_{0.6}O_{19-d}$), SrNi-3 ($Sr_{0.6}Ni_{0.4}Al_{11.6}Ni_{0.4}O_{19-d}$) and SrNi-4 ($Sr_{0.2}Ni_{0.8}Al_{12}O_{19-d}$) samples calcined at 1200°C were estimated in steam reforming of methane at 700°C. Figure 5 and Table 3 show these properties.

According to the obtained results, the gas contains residual methane and the reaction products CO, CO_2, H_2, and its amount is determined by the catalyst nature. Thus, together with SRM side WGS reaction gives a small amount of CO_2 products. This is consistent with the endothermic feature of the SRM reaction. The SRM activity increases with temperature [35]. Besides, WGS reaction is exothermic and reversible. The high temperature of the catalytic test shifts equilibrium of WGS reaction to the CO formation that leads to decrease of CO_2 concentration. The equilibrium composition of exit gases from steam reforming is determined by temperature, pressure and CH_4/H_2O ratio. Our reaction conditions are following H_2O/CH_4 = 2, p = 1.0 atm. Thus, according to calculations, the equilibrium concentration of methane is about 1.9% at the reaction temperature of 700°C.

Figure 5 shows the time dependence of product concentration over two samples: SrNi-2 and SrNi-4. It is seen (Figure 5a) that

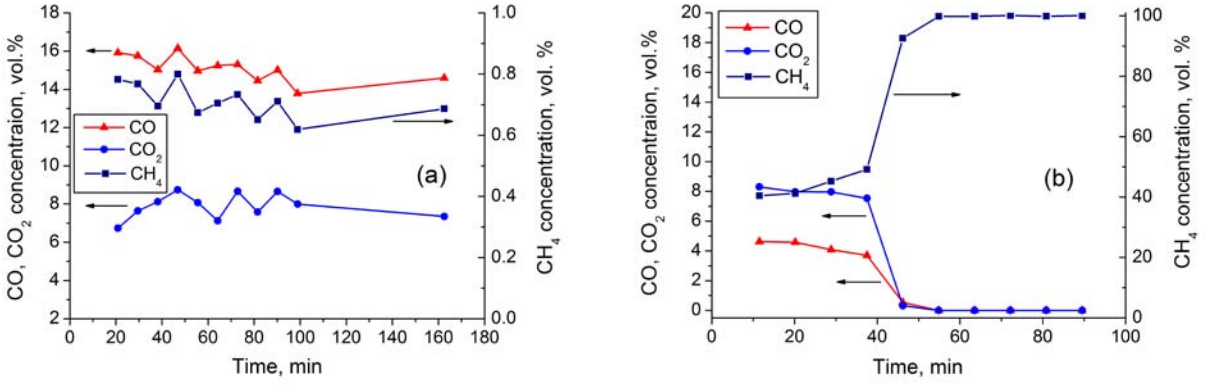

Figure 5. Catalytic stability of the (a) SrNi-2, (b) SrNi-4 catalysts at 700°C. H_2O/CH_4 = 2; flow rate 100 ml/min.

Table 3. Catalytic properties of the catalysts calcined at 1200°C.

Catalyst	700°C							
	Residual amount CH_4,		Reaction products					
			CO		CO_2		H_2	
	exp	*	Exp	*	exp	*	exp	*
	vol.%							
SrNi-1-1200	0.8±1.0	1.1	16.0±1.0	21.2	5.1±1.0	6.8	53.5±1.0	71.0
SrNi-2-1200	0.7±1.0	0.9	15.5±1.0	19.9	7.7±1.0	9.9	54.0±1.0	69.3
SrNi-3-1200	1.1±1.0	1.4	17.0±1.0	22.0	5.2±1.0	6.7	54.0±1.0	69.9
SrNi-4-1200	99.0±1.0	-	0	-	0	-	0	-
8 wt.% NiO/(Mg-Al-O-1200)	*1.9*	*2.5*	*16.2*	*21.4*	*6.3*	*8.3*	*51.0*	*67.7*
Equilibrium concentration		*1.9*		*16.1*		*6.8*		*75.2*

**calculations of the gas composition in dry mixture*

in the presence of the SrNi-2 sample, the residual amount of methane of 0.7 vol.% does not change for 160 minutes, CO and CO_2 concentration is 15.5 and 7.7 vol.%, respectively. At the same time, the amount of hydrogen formed is about 54.0 vol.%, which is significantly higher than concentration of CO and CO_2.

The other dependence is observed for the SrNi-4 sample (Figure 5b): at the initial moment, the residual amount of methane is 40 vol.%. The SrNi-4 catalyst contains $Ni_2Al_{18}O_{29}$ phase and, likely, a small amount of Sr-containing phase, nickel ions being located in a strongly bonded state, and are not reduced by hydrogen up to 900°C (Figure 3). It should be noted that the reaction was carried out to 700°C after sample reduction, so the concentration of metal nickel on the catalyst surface is low in SrNi-4 sample. Thus, the SrNi-4 catalyst is not very active.

The activity of the SrNi-4 sample decreases during reaction, and the catalyst becomes inactive after 50 minutes (the residual amount of methane is 100%). Observed decrease in activity is due to the relatively low amount of metal nickel (Figure 3, curve 3), which is coked rapidly. It is known that a side reaction proceeds with steam reforming simultaneously:

$$CH_4 \rightarrow C + 2H_2$$

It can be assumed that SrNi-4 catalyst which contains $Ni_2Al_{18}O_{29}$ phase with a high content of aluminum possesses high acidity, which provides the cracking of hydrocarbons. The catalytic properties of samples studied are given in Table 3. Thus, the activity estimated by the residual amount of methane is practically the same for the samples SrNi-1 ÷ SrNi-3 (*0.9 ÷ 1.4 vol.%*) and is essentially higher in comparison to the SrNi-4 (*99.0 vol.%*.) sample. Within uncertainty of analysis (±1.0 vol.% Table 3), conversion of methane over the first three samples is close to equilibrium one. Hence, activity of SrNi-1 – SrNi-3 samples are indiscernible within measurement accuracy. More detailed investigation of kinetics at shorter contact times will be given in future publications.

At the same time it is well-known that activity of Ni-containing catalysts in this reaction depends on particle size of metal nickel, which is formed during reduction of the samples. Comparison of catalyst activity in steam reformation of methane with H_2-TPR results reveals that the higher the reducibility of the catalyst, the higher its activity. It should be noted that prior reduction of the catalysts has been carried out at 900°C, while the reaction has been tested at 700°C. Hence, the metal nickel particles formed after reduction do not sinter at the reaction temperature. This activity is higher than that of a reference sample 8 wt.% Ni/Mg-Al-O (Table 3). It is noteworthy that the 8 wt.% Ni/Mg-Al-O sample is given in this paper as reference sample for studying dependence of catalytic properties of Ni-containing catalysts in steam reforming of methane on the nature of nickel species, supported or incorporated in the catalyst structure. According to Roh and et al. [36], the precipitated Ni-containing catalysts are more active than supported ones.

TEM results (Figure 6) for the reduced Ni/Mg-Al-O, and SrNi-2 samples confirm this statement. The support particles of the 8 wt.% Ni/Mg-Al-O sample are large and well-crystallized. Their shape is close to spherical one and the size of support particles ranges from 0.2 to 1 μm (Figure 6a). The size of the particles of supported component is in the range from 5 to 200 nm. Interplanar distances of supported particles determined by high resolution TEM images (Figure 6a, scale bar 5 nm) correspond to the phase of metal nickel (d_{111} = 0.203 nm, d_{200} = 0.176 nm, d_{220} = 0.124 nm, etc.). The Ni particles with size greater than 20 nm contain structural defects, such as twinning stripes (Figure 6a, scale bar 20 nm).

The oxide matrix of the SrNi-2 sample contains particles of two types: agglomerates of smaller particles of 50 nm (Figure 6b, region 1, the scale bar is 200 nm) and big crystallized particles of 200 nm - 1 μm (Figure 6b, region 2, the scale bar is 200 nm). The particle size of active component of this sample ranges from 5 to 30 nm, which is smaller than that of the Ni/Mg-Al-O sample. These particles are in the metal state. However, the particles differing by contrast are observed in TEM images. Figure 6b shows the portion of the sample with supported particles (regions 1 and 2, scale bar 20 nm). EDX spectra were taken from the regions 1 and 2 (Figure 6c,d). It is seen that in the case of metal particle (region 1) possessing a high contrast the intensive line of NiL and weak line of AlK from the oxide matrix are observed. For nickel particles with a lower contrast (Figure 6b, region 2) the less intensive line of NiL is observed (Figure 6d). Probably, decreased contrast and a lower ratio of Ni/Al in EDX spectra are related to the presence of nickel aluminate that is supported by the H_2-TPR data. The reduction is not complete at 900°C for the Ni-substituted Sr aluminate while the 8%Ni/Mg-Al-O sample is completely reduced at 600°C (figure is not shown). The particles of metal nickel are present on its surface.

Vedrine et al. [37] showed that reduction of Ni/Al_2O_3 can result in formation of two types of nickel particles: monodispersed epitaxially bonded nickel and metallic nickel. The first type is formed after reduction of nickel aluminate and the second type is formed after reduction of NiO. It can be assumed that these particles are present in the investigated catalysts, since the samples contain NiO and $NiAl_2O_4$ phases. For example, the ratio of particle types is determined by the catalyst nature. The strongly bonded nickel predominates in the SrNi-4 catalyst, and the amount of metal nickel is small.

Thus, the activity of the Ni-substituted hexaaluminates in steam reforming of methane depends on the different phase composition. The samples with predominate phase of hexaaluminate promoted by nickel displays a high activity exceeding that of the sample obtained by impregnating the support. The sample containing $Ni_2Al_{18}O_{29}$ phase is not active. Thus, catalytic properties of Ni-substituted hexaaluminates in steam reforming of methane is determined by substitution of Sr and/or Al by Ni.

The catalytic properties of samples do not depend on specific surface area that increases in the order: SrNi-1 (*11 m^2/g*) < SrNi-2 (*21 m^2/g*) » SrNi-3 (*20 m^2/g*) < SrNi-4 (*45 m^2/g*). However, the most active catalysts are the SrNi-1 ÷ SrNi-3 samples and the less active - SrNi-4.

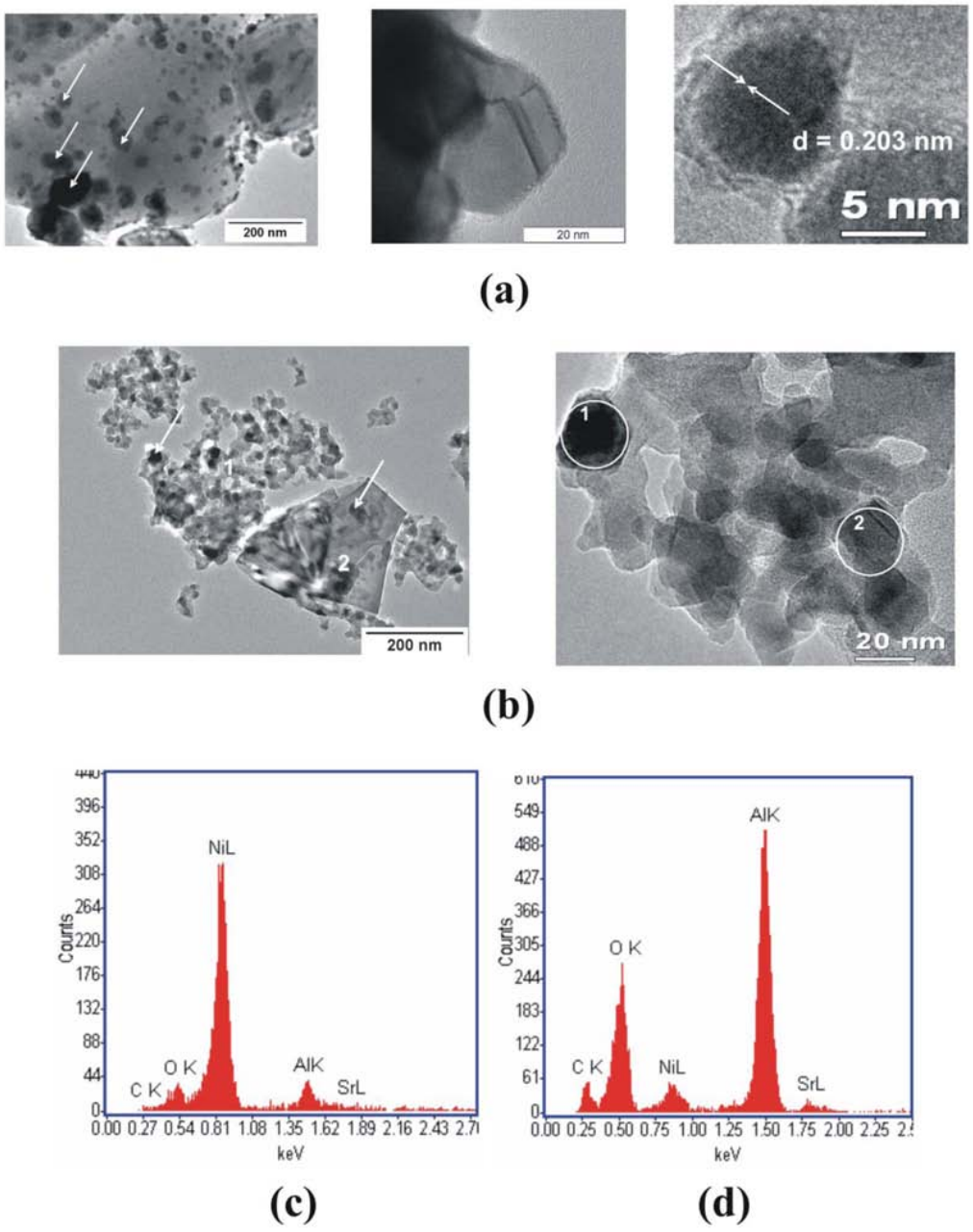

Figure 6. TEM images of the (a) 8%Ni/$MgAl_2O_4$ and (b) SrNi-2 samples. EDX data for regions 1 (c) and 2 (d) for the SrNi-2 sample.

4. Conclusions

The Ni-substituted catalysts $Sr_{1-x}Ni_xAl_{11.2+x}Ni_{0.8-x}O_{19}$ (x = 0; 0.2; 0.4; 0.8) obtained by precipitation and differing by content of nickel substituting Al and/or Sr ions in hexaaluminate structure have been investigated in steam reformation of methane. It has been shown that increasing *x* value results in change of phase composition. Transition from $SrAl_{11.2}Ni_{0.8}O_{19}$ to $Sr_{0.2}Ni_{0.8}Al_{12}O_{19}$ promotes destruction of hexaaluminate structure and formation of $Ni_2Al_{18}O_{29}$ phase which is not active in steam reformation of methane. According to XPS, nickel on the sample surface is Ni^{2+}, and its surface concentration is much lower than volume one that is evidence of its interaction with oxide composition. H_2-TPR data of the catalysts showed that the reduction in the temperature range of 30 – 900°C is not complete. However, the SrNi-2 sample possesses the highest reducibility and the SrNi-4 sample containing $Ni_2Al_{18}O_{29}$ phase, the lowest one, respectively. The high reducibility and high dispersion of the SrNi-2 catalyst determines its high activity in the steam reforming of methane since the active component is metal nickel and activity of the catalyst depends on its dispersion. On the other hand, high dispersion of metal nickel is related to the chosen object of investigation – Ni-substituted Sr hexaaluminates. Using Sr aluminate with the components ratio typical for hexaaluminate

structure in which nickel ions are homogeneously dispersed after treatment and reduction of the sample creates conditions for formation of highly dispersed and stable metal nickel particles on the catalyst surface. Thus the $Sr_{1-x}Ni_xAl_{11.2+x}Ni_{0.8-x}O_{19}$ (x = 0; 0.2; 0.4) catalysts are effective for steam reforming of methane.

Acknowledgements

The authors wish to thank kindly collaborators from Boreskov Institute of Catalysis: I.Yu. Molina for taking X-ray diffraction patterns and Irina A. Polukhina for catalytic tests.

References

[1] Salhi N., Boulahouache A., Petit C., Kiennemann A., Rabia C., Steam reforming of methane to syngas over $NiAl_2O_4$ spinel catalysts, Intern. J. Hydrogen Energy, 2011; 36, 11433 – 11439.

[2] Kim H.-W., Kang K.-M., Kwak H.-Y., Kim J. H., Preparation of supported Ni catalysts on various metal oxides with core/shell structures and their tests for the steam reforming of methane, Chem. Eng. J., 2011; 168, 775–783.

[3] Urasaki K., Sekine Y., Kawabe S., Kikuchi E., Matsukata M., Catalytic activities and coking resistance of Ni/perovskites in steam reforming of methane, Appl. Catal. A, 2005; 286, 23–29.

[4] Rostrup-Nielsen J.R., Bak-Hansen J.H., CO_2-Reforming of Methane over Transition Metals, J. Catal., 1993; 144, 38 – 49.

[5] Xu Z., Zhen M., Bi Y., Zhen K., Carbon dioxide reforming of methane to synthesis gas over hexaaluminate $ANiAl_{11}O_{19-d}$ (A = Ca, Sr, Ba and La) catalysts, Catal. Lett., 2000; 64, 157-161.

[6] Christensen K.O., Chen D., Lødeng R., Holmen A., Effect of supports and Ni crystal size on carbon formation and sintering during steam methane reforming, Appl. Catal. A, 2006; 314, 9–22.

[7] Gardner T.H., Shekhawat D., Berry D.A., Smith M.W., Salazar M., Kugler E.L., Effect of nickel hexaaluminate mirror cation on structure-sensitive reactions during *n*-tetradecane partial oxidation, Appl. Catal. A, 2007; 323, 1–8.

[8] Groppi G., Cristiani C., Forzatti P., $BaFe_xAl_{12-x}O_{19}$ system for high-temperature catalytic combustion, J. Catal., 1997; 168, 95-103.

[9] Takehira K., Highly dispersed and stable supported metal catalysts prepared by solid phase crystallization method, Catal. Surveys Japan, 2002; 6, 19-32.

[10] Reforming catalysts for ammonia production. Review of foreign literature, State institute of nitric industry, Moscow, 1989.

[11] Groppi G., Cristiani C., Forzatti P., Preparation, characterisation and catalytic activity of pure and substituted La-hexaaluminate systems for high temperature catalytic combustion, Appl. Catal. B, 2001; 35, 137-148.

[12] Lietti L., Cristiani C., Groppi G., Forzatti P., Preparation, characterization and reactivity of Me-hexaaluminate (Me = Mn, Co, Fe, Ni, Cr) catalysts in the catalytic combustion of NH_3-containing gasified biomasses, Catal. Today, 2000; 59, 191-204.

[13] Ivanova A.S., Zolotarsky I.A., Bobrova I.I., Smirnov E.I., Kuzmin V.A., Noskov A.S., Parmon V.N., Catalyst and preparation method of syngas of steam reforming of hydrocarbons, RF Patent № 2185239, Byull. Izobret., № 20 (2002).

[14] Price W.J., Analytical atomic-absorption spectroscopy, New York, 1976.

[15] Lowell S., Shields J.E., Thomas M.A., Thommes M., Characterization of Porous Solids and Powders: Surface Area, Pore Size and Density, Springer, Netherlands, 2006.

[16] Scofield J.H., Hartree-Slater subshell photoionization cross-sections at 1254 and 1487 eV, J. Electron Spectrosc. Relat. Phenom., 1976; 8, 129-137.

[17] Shirley D.A., High-Resolution X-Ray Photoemission Spectrum of the Valence Bands of Gold, Phys. Rev. B, 1972; 5, 4709-4714.

[18] Wang J., Tian Zh., Xu J., Xu Yu., Xu Zh., Lin L., Preparation of Mn substituted La-hexaaluminate catalysts by using supercritical drying, Catal. Today, 2003; 83, 213-222.

[19] Bukhtiyarova M.V., Ivanova A.S., Plyasova L.M., Litvak G.S., Budneva A.A., Paukshtis E.A., Structure and acid-base properties of hexaaluminates, React. Kinet. Catal. Lett., 2008; 93, 375 – 387.

[20] Scheffer B., Molhoek P., Moulijn J.A., Temperature-programmed reduction of $NiO-WO_3/Al_2O_3$ hydrodesulfurization catalysts, Appl. Catal., 1989; 46, 11-30.

[21] Chu W., Yang W., Lin L., The partial oxidation of methane to syngas over the nickel-modified hexaaluminate catalysts $BaNi_yAl_{12-y}O_{19-\square}$, Appl. Catal. A, 2002; 235, 39–45

[22] Roh H.-S., Jun K.-W., Dong W.-S., Baek S.-C., Park S.-E., Methane reforming reactions over stable Ni/q-Al_2O_3 catalysts, Journal Ind. Eng. Chem., 2002; 8, 464 – 471.

[23] Kosova N., Devyatkina E., Slobodyuk A., Kaichev V., Surface chemistry study of $LiCoO_2$ coated with alumina, Solid State Ionics, 2008; 179, 1745-1749

[24] Bukhtiyarova M.V., Ivanova A.S., Plyasova L.M., Litvak G.S., Rogov V.A., Kaichev V.V., Slavinskaya E.M., Kuznetsov P.A., Polukhina I.A., Selective catalytic reduction of nitrogen oxide by ammonia on Mn(Fe)-substituted Sr(La) aluminates, Appl. Catal. A, 2009; 357, 193-205.

[25] Sosulnikov M.I., Teterin Yu.A., X-ray photoelectron studies of Ca, Sr and Ba and their oxides and carbonates, J. Electron Spectrosc. Relat. Phenom., 1992; 59, 111 – 126.

[26] Dupin J.-C., Gonbeau D., Vinatier P., Levasseur A., Systematic XPS studies of metal oxides, hydroxides and peroxides, Phys. Chem. Chem. Phys., 2000; 2, 1319 – 1324.

[27] Van der Heide P.A.W., Photoelectron binding energy shifts observed during oxidation of group IIA, IIIA, IVA elemental surfaces, J. Electron Spectrosc. Relat. Phenom., 2006; 151, 79-91.

[28] Van Veenendaal M.A., Sawatzky G.A., Nonlocal screning effects in 2*p* x-ray photoemission spectroscopy core-level line shapes of transition metal compounds, Phys. Rev. Lett., 1993; 70, 2459-2462.

[29] McIntyre N.S., Cook M.G., X-ray photoelectron studies on some oxides and hydroxides of cobalt, nickel, and copper, Anal. Chem., 1975; 47, 2208-2213.

[30] Occelli M.L., Psaras D., Suib S.L., Stencel J.M., Metal contaminant effects on the properties of a silica-rich fluid cracking catalyst, Appl. Catal., 1986; 28, 143-160.

[31] Carley A.F., Jackson S.D., O'Shea J.N., Roberts M.W., The formation and characterization of Ni^{3+} – an x-ray photoelectron spectroscopic investigation of potassium-doped Ni(110)-O, Surf. Sci., 1999; 440, L868-L874.

[32] Chu Y., Li S., Lin J., Gu J., Yang Y., Partial oxidation of methane to carbon monoxide and hydrogen over $NiO/La_2O_3/g\text{-}Al_2O_3$, Appl. Catal. A, 1996; 134, 67 – 80.

[33] Machida M., Eguchi K., Arai H., Analytical electron microscope analysis of the formation of $BaO{\cdot}6Al_2O_3$, J. Amer. Cer. Soc., 1988; 71, 1142 – 1147.

[34] Xua Z., Zhen M., Bi Y., Zhena K., Catalytic properties of Ni modified hexaaluminates $LaNi_yAl_{12-y}O_{19}$ for CO_2 reforming of methane to synthesis gas, Appl. Catal. A, 2000; 198, 267 – 273.

[35] Huang T.-J., Huang M.-C., Effect of Ni content on hydrogen production via steam reforming of methane over Ni/GDC catalysts, Chem. Eng. J., 2008; 145, 149 – 153.

[36] Roh H.-S., Koo K.Y., Yoon W.L., Combined reforming of methane over co-precipitated Ni–CeO_2, Ni–ZrO_2 and Ni–$Ce_{0.8}Zr_{0.2}O_2$ catalysts to produce synthesis gas for gas to liquid (GTL) process, Catal. Today, 2009; 146, 71–75.

[37] Vedrine J.C., Hollinger G., Duc T.M., Investigation of antigorite and nickel supported catalysts by x-ray photoelectron spectroscopy, J. Phys. Chem., 1978; 82, 1515-1520